RSC Advances

PAPER

View Article Online
View Journal | View Issue

Cite this: *RSC Adv.*, 2019, **9**, 37733

Temperature modulation of defects in NH_2-UiO-66(Zr) for photocatalytic CO_2 reduction

Yanghe Fu,[a] Jieyu Wu,[a] Rongfei Du,[a] Ke Guo,[a] Rui Ma,[a] Fumin Zhang,[a] Weidong Zhu *[a] and Maohong Fan *[b]

Received 6th October 2019
Accepted 13th November 2019

DOI: 10.1039/c9ra08097j

rsc.li/rsc-advances

Defect engineering can be a promising approach to improve the photocatalytic performance of metal–organic frameworks (MOFs). Herein, a series of defective NH_2-UiO-66(Zr) materials were synthesized *via* simply controlling the synthesis temperature, with concentrated HCl as the modulator and then these as-prepared samples were used to systematically investigate the effects of their structural defects on photocatalytic CO_2 reduction. Remarkably, these MOFs with defects exhibit significantly enhanced activities in photocatalytic CO_2 reduction, compared with the material without defects. The defect engineering creates active binding sites and more open frameworks in the MOF, and thus facilitates the photo-induced charge transfer and restrains the recombination of photo-generated charges efficiently. The current work provides an instructive approach to improve the photocatalytic efficiency by taking advantage of the structural defects in MOFs, and could also inspire more work on the design of advanced defective MOFs.

Introduction

MOFs are an emerging class of porous materials constructed from metal-containing nodes (also known as secondary building units, or SBUs) and organic linkers, which have been extensively studied over the past two decades and shown a variety of applications.[1–3] In the skeleton of MOF materials the metal-oxo clusters could act as inorganic semiconducting quantum dots while the organic linkers serve as antennas to activate these semiconducting quantum dots by ligand-to-metal charge transfer (LMCT) upon photoexcitation, which makes MOF-based photocatalysis possible.[4] In addition, some functional MOFs are good at CO_2 capture due to their large surface area and tunable interactions with CO_2, especially facilitating the photocatalytic reduction of CO_2.[5] It is well known that the conversion of CO_2 into valuable chemicals and/or fuels utilizing solar energy is one of the most promising approaches to solve these problems associated with both global warming and energy shortage. Zirconium-based MOF UiO-66, based on $Zr_6O_4(OH)_4(CO_2)_{12}$ SBUs, has emerged as a promising platform for potential application in photocatalytic CO_2 reduction.[6,7] In its crystal structure, hexanuclear zirconium oxyhydroxide clusters are linked *via* terephthalate (1,4-benzenedicarboxylate, BDC) bridges to form a face-centered-cubic net that is notable for its high degree of topological connectivity (12 connected nodes),[8,9] a design feature considered responsible for its unusually high thermal and chemical stability. Like many other canonical MOFs, UiO-66 forms the basis of an isoreticular family, *i.e.*, Hf(IV), U(IV), Th(IV) or Ce(IV) can substitute Zr(IV),[10–13] and a number of different dicarboxylates can be used instead of BDC. For example, by substitution of BDC in UiO-66(Zr) with 2-aminoterephthalate anion (ATA), isostructural NH_2-UiO-66(Zr) can be obtained, and they have a photocatalytic activity in H_2 production and CO_2 reduction and can catalyze the transformation of various organic compounds into their corresponding oxygenated products upon visible-light irradiation.[14–18] However, their photocatalytic performance, especially in CO_2 reduction, is still not satisfactory due to the high recombination rate of the photo-induced charges.[19]

It has been recently reported that the defect engineering of MOFs can be a promising approach for tailoring their physicochemical properties such as stability, magnetism, gas adsorption, and catalytic activity.[20–25] It is common to use the concepts of heterogeneity and structural disorders of different nature interchangeably with the term "structural defects". UiO-66 has been considered as a model system, when one deals with defective MOFs, and two types of defects have been proposed to exist in its framework: missing-linker defects and missing-cluster defects.[20,26] Thereinto, the missing-linker defects incorporated by the so-called modulator approach can liberate Lewis acidic sites (Zr^{4+} sites with unsaturated coordination) and lead to a more open framework in UiO-66, providing novel opportunities for application in catalysis.[27–29] For example, the catalytic activity of defective UiO-66(Zr) for several Lewis acid catalyzed reactions can be drastically increased by the

[a]*Key Laboratory of the Ministry of Education for Advanced Catalysis Materials, Institute of Physical Chemistry, Zhejiang Normal University, Jinhua 321004, China. E-mail: weidongzhu@zjnu.cn*

[b]*Department of Chemical and Petroleum Engineering, University of Wyoming, Laramie, WY 82071, USA. E-mail: mfan@uwyo.edu*

combined use of trifluoroacetic acid and HCl during the synthesis, leading to the missing of the linkers.[27] In addition, it has been reported that the creating defects in UiO-66 *via* tuning the synthesis time is beneficial for the oxidation of dibenzothiophene.[28] These results have inspired further studies and at the same time raise the flag for the need of high-quality structural investigations on defective MOFs, based on both advanced experimental and computational simulation and modeling techniques. Presently, to our knowledge, research in the field of defect characterization and in turn the defect engineering of MOFs is empirical and function-driven while only a few studies have been focused on elucidating detailed structure–property relations guided by an atomistic and mesoscopic level of quantitative understanding. Moreover, the study of defect engineering as the way to improve the photocatalytic performance of MOFs is still rare.[30,31]

Herein, we wish to report a facile method to create defects in NH_2-UiO-66(Zr). *Via* simply tuning the crystallization temperature, a series of defective NH_2-UiO-66(Zr) samples were obtained in the present of hydrochloric acid as a modulator and then their photocatalytic activities in CO_2 reduction were also examined. In the current work, an attempt is to elucidate the effects of the introduced defects in the MOF on the photocatalysis in combination of advanced characterizations with the photocatalytic reaction and to open the possibility of using defect engineering as a new avenue to improve the photocatalytic performance involved with MOF-based materials.

Experimental

Chemicals

Zirconium(IV) chloride ($ZrCl_4$), 2-aminoterephthalic acid (H_2ATA), concentrated hydrochloric acid (HCl), *N*,*N*-dimethylformamide (DMF), sodium sulfate (Na_2SO_4), sodium carbonate (Na_2CO_3), sodium bicarbonate ($NaHCO_3$), and methanol (MeOH) were purchased from Aladdin Industrial Co. Triethanolamine (TEOA) and acetonitrile (MeCN) were purchased from Shanghai Chemical Reagent Co. All reagents were used as received without further purification.

Synthesis procedure

Defective NH_2-UiO-66(Zr). $ZrCl_4$ (0.250 g, 1.072 mmol) and H_2ATA (0.268 g, 1.483 mmol) were dissolved in anhydrous DMF (50 mL) at room temperature. Concentrated hydrochloric acid (10 mL) was added to the mixture. Then the obtained mixture was stirred for 30 min and transferred into a 100 mL Teflon-lined stainless steel autoclave and heated for 24 h at the desired temperature. The final product was filtered, washed with DMF and methanol, extracted in a Soxhlet extractor with methanol, and vacuum-dried at 353 K. The obtained samples were named as Zr-MOF-*T* (T = 353 K, 393 K, 433 K, and 473 K, respectively).

Defect-free NH_2-UiO-66(Zr). $ZrCl_4$ (0.250 g, 1.072 mmol) and H_2ATA (0.268 g, 1.483 mmol) were dissolved in anhydrous DMF (50 mL), then 0.15 mL deionized water was added. Afterwards, the above mixture was stirred at room temperature for 30 min and transferred into a 100 mL Teflon-lined stainless steel autoclave and heated at 473 K for 24 h in an oven. The obtained sample was named as Zr-MOF-DF (DF: defect-free).

Characterization

The powder X-ray diffraction (XRD) patterns were collected on a D8 Advance X-ray diffractometer (Bruker) using Cu Kα radiation (λ = 0.1541 nm) in a scanning range of 3–50° at 2° min^{-1}. The textural properties of the prepared samples were determined by N_2 adsorption/desorption at 77 K using an ASAP 2020 apparatus (Micromeritics Instrument Corp.). The samples were degassed in vacuum at 453 K for 15 h prior to adsorption measurement. The thermogravimetric analysis (TGA) was performed in flowing air on a STA-449C instrument (Netzsch) with a heating rate of 5 K min^{-1}. The Fourier transform infrared (FT-IR) spectra were recorded on a Nicolet NEXUS670 spectrometer (ThermoFisher) with a resolution of 4 cm^{-1}. The UV-vis diffuse reflectance spectra (UV-vis DRS) were recorded on a Nicolet Evolution 500 Spectrophotometer (ThermoFisher) with $BaSO_4$ as reflectance standard from 200 to 800 nm. The scanning electron microscope (SEM) was carried out on a S-4800 apparatus (Hitachi) equipped with a field emission gun. The X-ray photoelectron spectroscopy (XPS) was carried out on Thermo Scientific EscaLab 250Xi using Al Kα radiation (ThermoFisher). The photoluminescence (PL) spectra were recorded on a F-7000 spectrometer (Hitachi) excited at 326 nm. The photocurrent (PC) analysis was carried out with a CHI760E workstation (Shanghai Chenhua Instruments Co.) in a conventional three-electrode cell using a Pt plate and an Ag/AgCl electrode as the counter electrode and reference electrode, respectively. The photocatalyst powder deposited on the fluoride tin oxide (FTO) substrate was employed as the working electrode and a quartz cell filled with 100 mL 0.2 M Na_2SO_4 electrolyte was used as the reaction system. A 300 W PLS-SXE 300D xenon lamp (Beijing Perfectlight) system was applied as the excitation light source equipped with a UV cutoff filter and an IR-cut filter, which was the same light source for the photocatalytic reactions.

Photocatalytic reaction

Prior to reactions, the photocatalysts were treated under vacuum at 453 K to remove any adsorbed impurities. After the photocatalyst (50 mg) was added into a reaction flask, it was degassed and purged with CO_2. A mixture of MeCN and TEOA (60 mL in total) with a volume ratio of 5 to 1 was degassed by CO_2 to remove dissolved O_2, and then injected into the reaction flask. The photocatalytic reaction was carried out under the irradiation of a 300 W Xe lamp with a UV-cut filter and an IR-cut filter (800 nm $\geq \lambda \geq$ 420 nm) for 10 h. The formed HCOOH was detected by an ion chromatography (930 Compact IC pro, Metrosep) with a Metrosep A supp 5250/4.0 column. A mixture of 3.2 mM Na_2CO_3 and 1.0 mM $NaHCO_3$ was used as eluent. The gaseous reaction products were also analysed using a GC (Agilent 6890A) with a HP-5 capillary column for flame ionization detector (FID) and a 5A molecular sieve packed column for thermal conductivity detector (TCD). For the reusability test, after the reaction, the photocatalyst was separated from the

reaction medium, repeatedly washed with MeOH twice, and then dried overnight in a vacuum oven at 453 K.

Results and discussion

NH_2-UiO-66(Zr) samples with tunable defects were synthesized from a mixture containing $ZrCl_4$ and H_2ATA in DMF, with the addition of concentrated HCl as the modulator at different reaction temperatures. For comparison, the near defect-free NH_2-UiO-66 was prepared according to the previously reported procedure with slight modification.[32] As shown in Fig. 1, the XRD patterns of Zr-MOF-*T* (*T* from 353 to 473 K) and Zr-MOF-DF suggest a highly crystalline nature and are in good agreement with the simulated pattern reported in the literature,[8] revealing maintenance of the cubic close packed structure of NH_2-UiO-66(Zr) during the defect formation, even though the concentrated HCl was used in the preparation. However, a very broad peak in the low-angle region (3–7°, 2θ) can be observed in the XRD patterns of the defective samples by comparing with that of Zr-MOF-DF, indicating the presence of defect nanoregions (inset in Fig. 1).[22,33,34] Furthermore, the relative intensity of the broad peak, correlated with the concentration of these defects, increases with increasing the crystallization temperature. However, the XRD pattern of Zr-MOF-483 K shows an amorphous phase, implying that the framework of the MOF will be collapsed, when the synthesis temperature is above 473 K. The obtained samples were further investigated by SEM to examine their morphologies. As seen in Fig. 2, the defective Zr-MOF-*T* samples possess a relatively low crystallinity with irregular shaped particles in comparison with Zr-MOF-DF that shows octahedral crystals without apparent surface defects. The adsorption isotherms of N_2 on the five synthesized samples at 77 K are shown in Fig. 3. It is known that the calculated geometric surface area of a defect-free NH_2-UiO-66(Zr) with 12 linkers per node is 700 $m^2\ g^{-1}$.[35] As can be seen, the Brunauer–Emmett–Teller (BET) surface areas of the defective samples are larger than that of the defect-free one and of the theoretically

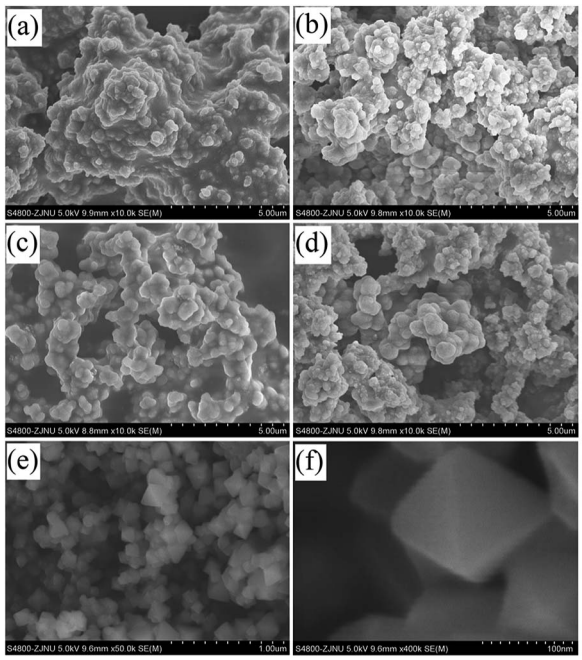

Fig. 2 SEM images of Zr-MOF-353 K (a), Zr-MOF-393 K (b), Zr-MOF-433 K (c), Zr-MOF-473 K (d), and Zr-MOF-DF (e and f).

calculated one and continuously increase with increasing the crystallization temperature. Zr-MOF-473 K, for example, exhibits the largest BET surface area (1133 $m^2\ g^{-1}$) and pore volume (0.63 $cm^3\ g^{-1}$), about 49% and 65% higher than the corresponding values of Zr-MOF-DF (758 $m^2\ g^{-1}$ and 0.38 $cm^3\ g^{-1}$, shown in Table 1), implying that a higher crystallization temperature results in more vacancies in the MOF. The pore size distributions of Zr-MOF-*T* samples (inset in Fig. 3) obtained by the density functional theory (DFT) calculation show three maxima at *ca.* 0.8, 1.2, and 1.5 nm, which can be interpreted as the tetrahedral cages, the octahedral cages and/or the tetrahedral cages with missing linkers, and the octahedral cages with

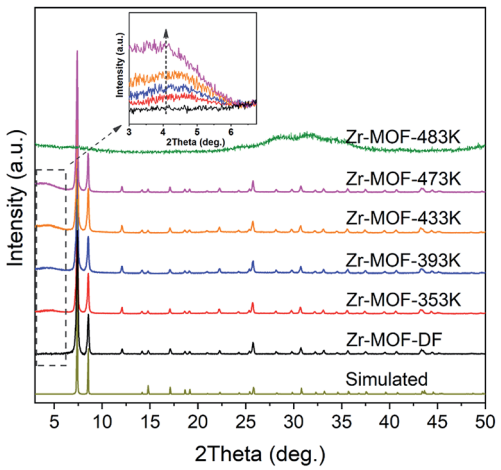

Fig. 1 XRD patterns of Zr-MOF-*T* and Zr-MOF-DF samples. The inset shows the low-angle (2θ = 3–7°) region of the obtained XRD patterns.

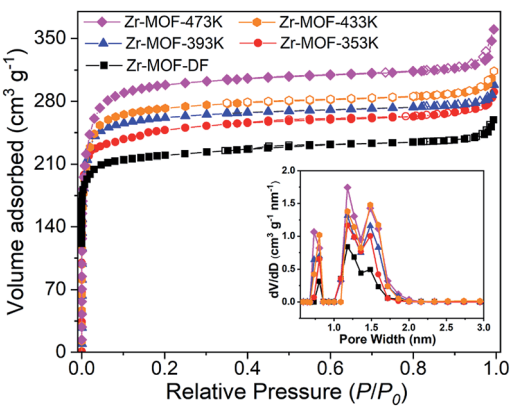

Fig. 3 Adsorption–desorption isotherms of N_2 on Zr-MOF-*T* and Zr-MOF-DF samples at 77 K. The inset shows the pore-size distributions for the prepared samples extracted from the N_2 adsorption isotherms calculated by DFT.

Table 1 BET surface areas and pore volumes of Zr-MOF-DF and Zr-MOF-*T* samples

Sample	S_{BET} (m^2 g^{-1})	V_{total}[a] (cm^3 g^{-1})
Zr-MOF-DF	778	0.38
Zr-MOF-353 K	915	0.46
Zr-MOF-393 K	982	0.51
Zr-MOF-433 K	1028	0.54
Zr-MOF-473 K	1133	0.63

[a] Single point adsorption total pore volume at $P/P_0 = 0.985$.

missing linkers and/or the defect-related nano-regions, respectively.[35,36]

The TGA results might provide some quantitative information on structural defects. It is well known that the structural unit of a defect-free NH_2-UiO-66(Zr) is $Zr_6O_4(OH)_4(ATA)_6$. Upon heat treatment, the removal of the solvent and the dehydroxylation of the Zr_6 cluster would be completed at about 550 K, giving an inner cluster of $Zr_6O_6(ATA)_6$.[37] The decomposition of the ATA linkers occurs at about 573 K, finally forming the only solid product of ZrO_2 in air atmosphere. Thus the weight at about 573 K for $Zr_6O_6(ATA)_6$ should ideally reach 232% when normalized to the final end weight as 100%. As shown in Fig. 4, the normalized weight at about 573 K for the near defect-free Zr-MOF-DF sample (235%) is in good agreement with the theoretical value while the ones for all the Zr-MOF-*T* samples are clearly below the theoretical value, indicating that the obtained defective samples possess abundant missing-linker defects. The apparent concentrations of the missing-linker defects in Zr-MOF-*T* (*T* from 353 to 473 K) are estimated to be 11%, 17%, 19%, and 22%, respectively. These values are probably overestimated due to the fact that the missing metal-cluster defects likely coexist in the defective Zr-MOFs. However, it holds the general trend that the degree of the defects increases with increasing the crystallization temperature during the synthesis.

Considering all the above, it is apparent that the defective Zr-MOFs were successfully prepared and the linker deficiencies can be tailored by controlling the synthesis temperature with concentrated HCl as the modulator. Differently, a high synthesis temperature can lead to the formation of a defect-free UiO-66.[38] This difference might be related to the presence of amino group on the organic linker 2-aminoterephthalic acid used in the current study but a clear explanation cannot be given at this moment. During crystal formation, HCl counteracts the deprotonation of the dissolved carboxylic acids and favors the competitive incorporation of ATA with increasing temperature, leading to the formation of inherent defects either from misconnections or dislocations during the crystallization of Zr-MOFs.[27,36,39] However, an amorphous phase will be formed, when the synthesis temperature is above 473 K, leading to the collapse of Zr-MOF framework due to the corrosivity of concentrated HCl, especially for the amine-functionalized UiO-66.

To study the influence of structural defects on photocatalysis, photocatalytic CO_2 reduction was performed using TEOA as the sacrificial agent upon visible-light irradiation, and these results are shown in Fig. 5. All the defective Zr-MOF-*T* samples exhibit photocatalytic activities in CO_2 reduction and their activities increase expectedly with increasing the synthesis temperature. For example, Zr-MOF-473 K displays the highest activity with about 129.8 μmol g_{cat}^{-1} h^{-1} of the HCOOH produced in 10 h irradiation, much higher than that of Co-doped NH_2-MIL-125(Ti) (38.4 μmol g_{cat}^{-1} h^{-1}).[40] Moreover, the photocatalytic performance of the defect-free MOF was also investigated and its activity is significantly lower, compared to those of Zr-MOF-*T* samples. This indicates that the defects in NH_2-UiO-66(Zr) play an important role in photocatalytic CO_2 reduction. In addition, a five-run experiment of photocatalytic CO_2 reduction over Zr-MOF-473 K was carried out to check the reusability (Fig. 6). Obviously, the recycling use of the photocatalyst for five runs shows no obvious decrease in the photocatalytic activity. The XRD and FT-IR characterization results for the used photocatalyst after the 5th-run reaction are almost identical to those for the fresh one (Fig. 7), suggesting that the prepared catalyst is stable enough during the photocatalytic reaction.

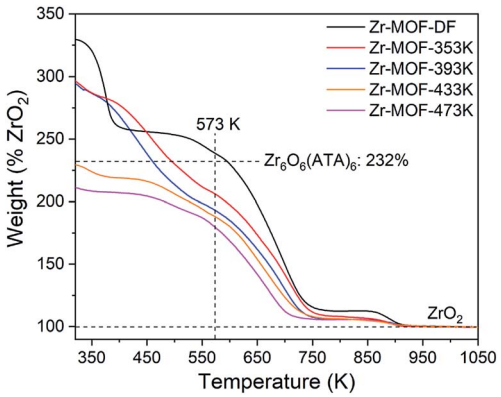

Fig. 4 TGA curves of Zr-MOF-*T* and Zr-MOF-DF samples.

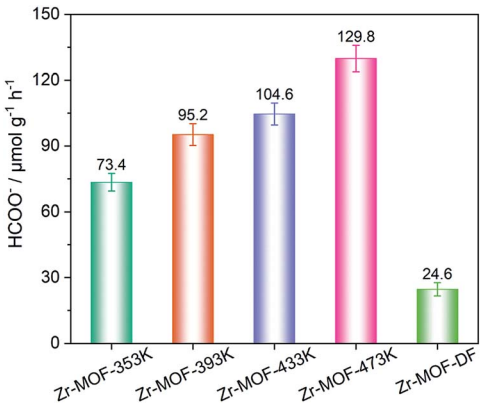

Fig. 5 Amount of the produced HCOOH over Zr-MOF-*T* and Zr-MOF-DF samples upon visible-light irradiation (800 nm ≥ λ ≥ 420 nm). Photocatalyst: 50 mg, MeCN/TEOA volume ratio: 5/1, total solution volume: 60 mL.

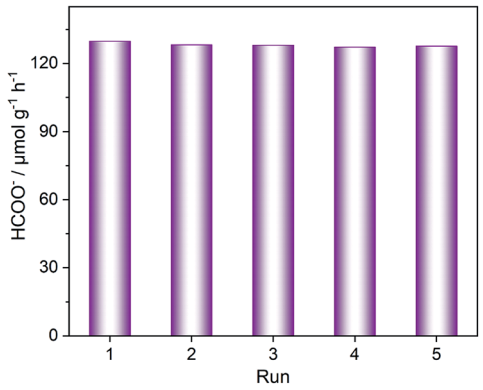

Fig. 6 Reusability of Zr-MOF-473 K in CO_2 reduction upon visible-light irradiation.

In theory, missing-linker defects will result in a change of the environment of the affected Zr atoms, which often lowers their unoccupied d orbitals and increases charge transfer likelihood, therefore, improving the photocatalytic activity.[29] To verify this, the PL and PC experiments were further carried out to investigate the photogenerated charge separation efficiency of the defective samples. As shown in Fig. 8, the PL spectra of Zr-MOF samples exhibit an emission peak at around 480 nm when excited at 326 nm. Such a peak is greatly weakened with an increase in the structural defects with increasing the synthesis temperature, indicating that the defective Zr-MOFs can

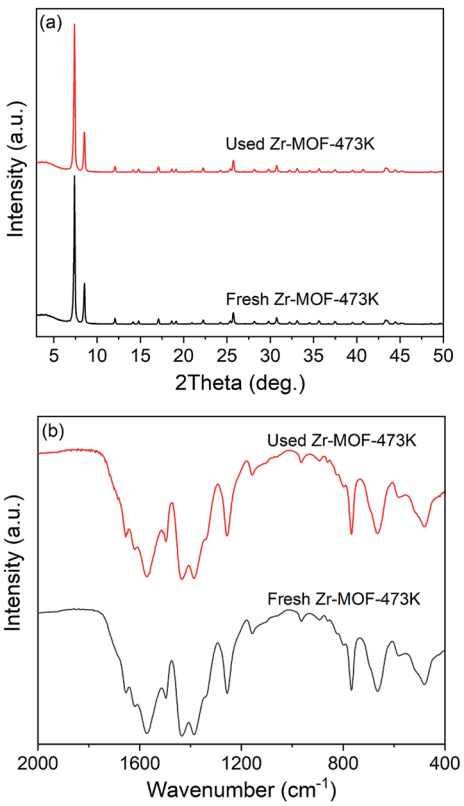

Fig. 7 XRD patterns (a) and IR spectra (b) of the fresh and used Zr-MOF-473 K.

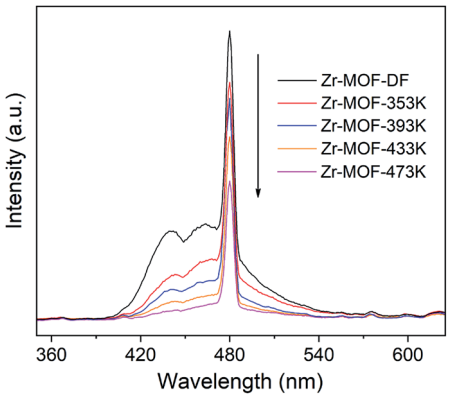

Fig. 8 Photoluminescence spectra of Zr-MOF-*T* and Zr-MOF-DF samples excited at 326 nm.

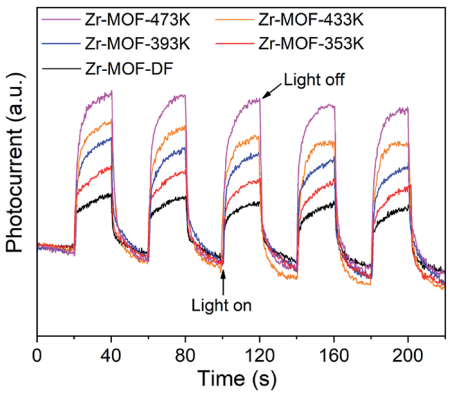

Fig. 9 Transient photocurrent responses of Zr-MOF-*T* and Zr-MOF-DF samples in 0.2 M Na_2SO_4 aqueous solution upon visible-light irradiation (800 nm $\geq \lambda \geq$ 420 nm).

significantly prohibit the recombination of the photo-generated charge. The transient photocurrent density responses of the photocatalysts in an on–off cycle mode are shown in Fig. 9. Upon visible-light irradiation, all the defective Zr-MOF catalysts show much higher photoelectric currents in comparison with Zr-MOF-DF, among which Zr-MOF-473 K exhibits the highest photocurrent response. Based on these results, it can be inferred that the effects of the structural defects on the ligand-to-metal charge transition are highly dependent on the number of defects and their configuration. For a sufficient number of the missing linkers, the defects in Zr-MOFs will facilitate the photo-induced charge transfer and restrain the recombination of photo-generated charge efficiently, which is beneficial for further photocatalytic steps.

Conclusions

In summary, the defective Zr-MOFs were successfully prepared and the linker deficiencies can be tailored *via* simply controlling the synthesis temperature with concentrated HCl as the modulator. Compared to the defect-free MOF, the defective ones exhibit significantly enhanced activities in photocatalytic CO_2 reduction. This defect engineering creates the active

binding sites and more open frameworks in the MOF, thus facilitates the photo-induced charge transfer and restrains the recombination of photo-generated charge efficiently, resulting in a higher photocatalytic activity.

Conflicts of interest

There are no conflicts to declare.

Acknowledgements

This work is financially supported by Zhejiang Provincial Natural Science Foundation of China (LY18B030006 and LY18B060006), National Natural Science Foundation of China (21476214, 21576243, 21303166, and 21706239), and the Programme of Introducing Talents of Discipline to Universities (D17008).

Notes and references

1 H. Furukawa, K. E. Cordova, M. O'Keeffe and O. M. Yaghi, *Science*, 2013, **341**, 1230444.
2 P. Silva, S. M. F. Vilela, J. P. C. Tomé and F. A. A. Paz, *Chem. Soc. Rev.*, 2015, **44**, 6774–6803.
3 B. Li, H.-M. Wen, Y. Cui, W. Zhou, G. Qian and B. Chen, *Adv. Mater.*, 2016, **28**, 8819–8860.
4 T. Tachikawa, J. R. Choi, M. Fujitsuka and T. Majima, *J. Phys. Chem. C*, 2008, **112**, 14090–14101.
5 Y. Chen, D. Wang, X. Deng and Z. Li, *Catal. Sci. Technol.*, 2017, **7**, 4893–4904.
6 Y. Bai, Y. Dou, L.-H. Xie, W. Rutledge, J.-R. Li and H.-C. Zhou, *Chem. Soc. Rev.*, 2016, **45**, 2327–2367.
7 D. Sun and Z. Li, *Chin. J. Chem.*, 2017, **35**, 135–147.
8 J. H. Cavka, S. Jakobsen, U. Olsbye, N. Guillou, C. Lamberti, S. Bordiga and K. P. Lillerud, *J. Am. Chem. Soc.*, 2008, **130**, 13850–13851.
9 M. J. Cliffe, W. Wan, X. Zou, P. A. Chater, A. K. Kleppe, M. G. Tucker, H. Wilhelm, N. P. Funnell, F.-X. Coudert and A. L. Goodwin, *Nat. Commun.*, 2014, **5**, 4176.
10 S. Jakobsen, D. Gianolio, D. S. Wragg, M. H. Nilsen, H. Emerich, S. Bordiga, C. Lamberti, U. Olsbye, M. Tilset and K. P. Lillerud, *Phys. Rev. B: Condens. Matter Mater. Phys.*, 2012, **86**, 125429.
11 C. Falaise, C. Volkringer, J. F. Vigier, N. Henry, A. Beaurain and T. Loiseau, *Chem.–Eur. J.*, 2013, **19**, 5324–5331.
12 C. Falaise, J. S. Charles, C. Volkringer and T. Loiseau, *Inorg. Chem.*, 2015, **54**, 2235–2242.
13 M. Lammert, M. T. Wharmby, S. Smolders, B. Bueken, A. Lieb, K. A. Lomachenko, D. D. Vos and N. Stock, *Chem. Commun.*, 2015, **51**, 12578–12581.
14 D. Sun, Y. Fu, W. Liu, L. Ye, D. Wang, L. Yang, X. Fu and Z. Li, *Chem.–Eur. J.*, 2013, **19**, 14279–14285.
15 A. S. Portillo, H. G. Baldoví, M. T. G. Fernandez, S. Navalón, P. Atienzar, B. Ferrer, M. Alvaro, H. Garcia and Z. Li, *J. Phys. Chem. C*, 2017, **121**, 7015–7024.
16 D. Sun and Z. Li, *J. Phys. Chem. C*, 2016, **120**, 19744–19750.
17 S. Wang and X. Wang, *Small*, 2015, **11**, 3097–3112.
18 R. Li, W. Zhang and K. Zhou, *Adv. Mater.*, 2018, **30**, 1705512.
19 A. Dhakshinamoorthy, Z. Li and H. Garcia, *Chem. Soc. Rev.*, 2018, **47**, 8134–8172.
20 Z. Fang, B. Bueken, D. E. D. Vos and R. A. Fischer, *Angew. Chem., Int. Ed.*, 2015, **54**, 7234–7254.
21 J. Ren, M. Ledwaba, N. M. Musyoka, H. W. Langmi, M. Mathe, S. Liao and W. Pang, *Coord. Chem. Rev.*, 2017, **349**, 169–197.
22 G. C. Shearer, S. Chavan, S. Bordiga, S. Svelle, U. Olsbye and K. P. Lillerud, *Chem. Mater.*, 2016, **28**, 3749–3761.
23 R. C. Klet, Y. Liu, T. C. Wang, J. T. Hupp and O. K. Farha, *J. Mater. Chem. A*, 2016, **4**, 1479–1485.
24 L. Yuan, M. Tian, J. Lan, X. Cao, X. Wang, Z. Chai, J. K. Gibsone and W. Shi, *Chem. Commun.*, 2018, **54**, 370–373.
25 H. Wu, Y. S. Chua, V. Krungleviciute, M. Tyagi, P. Chen, T. Yildirim and W. Zhou, *J. Am. Chem. Soc.*, 2013, **135**, 10525–10532.
26 S. Dissegna, K. Epp, W. R. Heinz, G. Kieslich and R. A. Fischer, *Adv. Mater.*, 2018, **30**, 1704501.
27 F. Vermoortele, B. Bueken, G. l. L. Bars, B. V. d. Voorde, M. Vandichel, K. Houthoofd, A. Vimont, M. Daturi, M. Waroquier, V. V. Speybroeck, C. Kirschhock and D. E. D. Vos, *J. Am. Chem. Soc.*, 2013, **135**, 11465–11468.
28 W. Xiao, Q. Dong, Y. Wang, Y. Li, S. Deng and N. Zhang, *CrystEngComm*, 2018, **20**, 5658–5662.
29 A. D. Vos, K. Hendrickx, P. V. D. Voort, V. V. Speybroeck and K. Lejaeghere, *Chem. Mater.*, 2017, **29**, 3006–3019.
30 X. Ma, L. Wang, Q. Zhang and H.-L. Jiang, *Angew. Chem., Int. Ed.*, 2019, **58**, 12175–12179.
31 M. Taddei, G. M. Schukraft, M. E. A. Warwick, D. Tiana, M. J. McPherson, D. R. Jones and C. Petit, *J. Mater. Chem. A*, 2019, **7**, 23781–23786.
32 M. Kandiah, M. H. Nilsen, S. Usseglio, S. Jakobsen, U. Olsbye, M. Tilset, C. Larabi, E. A. Quadrelli, F. Bonino and K. P. Lillerud, *Chem. Mater.*, 2010, **22**, 6632–6640.
33 C. Atzori, G. C. Shearer, L. Maschio, B. Civalleri, F. Bonino, C. Lamberti, S. Svelle, K. P. Lillerud and S. Bordiga, *J. Phys. Chem. C*, 2017, **121**, 9312–9324.
34 Y. Chiang, S. Bhattacharyya, K. C. Jayachandrababu, R. P. Lively and S. Nair, *ACS Sustainable Chem. Eng.*, 2018, **6**, 7931–7939.
35 M. J. Katz, Z. J. Brown, Y. J. Colón, P. W. Siu, K. A. Scheidt, R. Q. Snurr, J. T. Hupp and O. K. Farha, *Chem. Commun.*, 2013, **49**, 9449–9451.
36 W. Liang, C. J. Coghlan, F. Ragon, M. Rubio-Martinez, D. M. D'Alessandro and R. Babarao, *Dalton Trans.*, 2016, **45**, 4496–4500.
37 A. Schaate, P. Roy, A. Godt, J. Lippke, F. Waltz, M. Wiebcke and P. Behrens, *Chem.–Eur. J.*, 2011, **17**, 6643–6651.
38 G. C. Shearer, S. Chavan, J. Ethiraj, J. G. Vitillo, S. Svelle, U. Olsbye, C. Lamberti, S. Bordiga and K. P. Lillerud, *Chem. Mater.*, 2014, **26**, 4068–4071.
39 M. Vandichel, J. Hajek, F. Vermoortele, M. Waroquier, D. E. D. Vos and V. V. Speybroeck, *CrystEngComm*, 2015, **17**, 395–406.
40 Y. Fu, H. Yang, R. Du, G. Tu, C. Xu, F. Zhang, M. Fan and W. Zhu, *RSC Adv.*, 2017, **7**, 42819–42825.

